

# Ring cycle for dilating and constricting the nuclear pore

Sozanne R. Solmaz<sup>1</sup>, Günter Blobel<sup>1</sup>, and Ivo Melčák<sup>1</sup>

Laboratory of Cell Biology, Howard Hughes Medical Institute, The Rockefeller University, New York, NY 10065

Contributed by Günter Blobel, February 8, 2013 (sent for review January 31, 2013)

We recently showed that the three “channel” nucleoporins, Nup54, Nup58, and Nup62, interact with each other through only four distinct sites and established the crystal structures of the two resulting “interactomes,” Nup54•Nup58 and Nup54•Nup62. We also reported instability of the Nup54•Nup58 interactome and previously determined the atomic structure of the relevant Nup58 segment by itself, demonstrating that it forms a twofold symmetric tetramer. Here, we report the crystal structure of the relevant free Nup54 segment and show that it forms a tetrameric, helical bundle that is structurally “conditioned” for instability by a central patch of polar hydrogen-bonded residues. Integrating these data with our previously reported results, we propose a “ring cycle” for dilating and constricting the nuclear pore. In essence, three homooligomeric rings, one consisting of eight modules of Nup58 tetramers, and two, each consisting of eight modules of Nup54 tetramers, are stacked in midplane and characterize a constricted pore of 10- to 20-nm diameter. In going to the dilated state, segments of one Nup58 and two Nup54 tetrameric modules reassort into a dodecameric module, eight of which form a single, heterooligomeric midplane ring, which is flexible in a diameter range of 40–50 nm. The ring cycle would be regulated by phenylalanine-glycine regions (“FG repeats”) of channel nups. Akin to ligand-gated channels, the dilated state of the midplane ring may be stabilized by binding of [cargo•transport-factor] complexes to FG repeats, thereby linking the ratio of constricted to dilated nuclear pores to cellular transport need.

ligand gating | X-ray crystallography | nucleo-cytoplasmic transport

In evolution from prokaryotes to eukaryotes, the myriad of reactions yielding cotranscriptional and posttranscriptional assembly of ribonucleoproteins was largely confined to the nuclear compartment. This required the concomitant evolution of transport conduits of a sufficiently large diameter to allow passage of assembled ribonucleoproteins to the cytoplasm. Among these, newly assembled ribosomal subunits presented a special challenge, as they are relatively rigid bodies; the eukaryotic large ribosomal subunit, for example, has a diameter of about 30 nm. Hence, a correspondingly large nuclear pore had to evolve to accommodate the passage of ribosomal subunits, but also to protect against concomitant bidirectional leakage of the myriad of proteins, which are generally much smaller than ribonucleoproteins, to help maintain distinct nucleoplasmic and cytoplasmic proteomes. One way for meeting the challenge to transport diverse substrates of a large size range would be to endow the nuclear pore with the ability to have its central transport channel undergo dilation and constriction. However, as has been argued elsewhere (1), diameter changes in the 30-nm range might buckle the membrane, if channel proteins were directly embedded into the membrane’s lipid bilayer. It could be conjectured that evolution of the nuclear pore into the massive protein complex of over 100 MDa in vertebrates (reviewed in ref. 2), was in part dictated by the need to cushion the huge diameter changes of a central transport channel by a large and deformable surrounding protein matrix.

The concept of a dilatable pore in a deformable protein matrix is supported by electron-microscopic studies (3–5). Considerable shape and diameter changes of the central transport conduit have been reported. However, the resolution, even of the most

recently published cryo-electron tomography images, 60 Å at best (2), is not sufficient to yield insight into how such plasticity could be achieved at the molecular level. Likewise, a low-resolution, computational model, suggesting location probabilities of the multiple copies of the about 30 distinct nucleoporins within the nuclear pore complex (NPC) (6), does not address how the plasticity that was detected by electron microscopy could be achieved. In this model, the 30 nups of the yeast NPC essentially form a highly linked scaffold, where multiple copies of about 16 distinct nups delimit a central transport conduit, whereas other nups provide anchorage to specific integral membrane proteins in the curved pore membrane. In the computational as well as several other current models, key aspects of NPC function are not controlled by dilation and constriction of a central transport channel, but are collectively delegated instead to natively unstructured, phenylalanine-glycine (FG repeat)-containing regions, present in about a third of the nups (reviewed in ref. 7). Projecting from the scaffold to the center as well as to the cytoplasmic and nucleoplasmic side of the central transport conduit, these FG repeats have a dual function: to capture [cargo•transport-factor] complexes for transport across the central transport conduit (8) and, in an unoccupied state, to also form a permeability barrier (7).

This widely held view of nups merely forming a static transport conduit strategically placing those nups containing FG repeats to exert their dual function, has recently been challenged by studies on the structured regions of three centrally localized nups (9, 10), Nup58, Nup54, and Nup62, collectively referred to as “channel nups” (11, 12). From mapping and crystallographic analyses of interacting fragments of channel nups, we pieced together a molecular model for the central transport channel of the nuclear pore complex (12). The salient feature of this model is a single and flexible midplane ring, 40–50 nm in diameter, representing a “dilated” (open, active) form of the central transport channel. Remarkably, this large midplane ring is built from only two distinct segments of Nup54 and Nup58. These segments assemble to a dodecamer module composed of four segments of Nup58 and eight segments of Nup54. Eight dodecamers form the dilated ring. As the dodecamer displays dynamic instability, its constituent segments can segregate into three homotetrameric modules, two containing Nup54 and one of Nup58 (12). We already showed that the relevant Nup58 fragment by itself forms a twofold symmetric homotetramer (11) and proposed that eight such Nup58 homotetramers assemble into a midplane ring embodying part of a constricted (closed, inactive) form of the transport channel, about 20 nm in diameter (12). However, the fate of the relevant Nup54 segments following transition from a dilated to a constricted form of the midplane ring was heretofore unknown.

Author contributions: S.R.S., G.B., and I.M. designed research; S.R.S. and I.M. performed research; S.R.S., G.B., and I.M. analyzed data; and S.R.S., G.B., and I.M. wrote the paper. The authors declare no conflict of interest.

Freely available online through the PNAS open access option.

Data deposition: The atomic coordinates and structure factors have been deposited in the Protein Data Bank, [www.pdb.org](http://www.pdb.org) (PDB ID code 4J3H).

<sup>†</sup>To whom correspondence may be addressed. E-mail: [blobel@rockefeller.edu](mailto:blobel@rockefeller.edu), [ssolmaz@rockefeller.edu](mailto:ssolmaz@rockefeller.edu), or [melcaki@rockefeller.edu](mailto:melcaki@rockefeller.edu).

This article contains supporting information online at [www.pnas.org/lookup/suppl/doi:10.1073/pnas.1302655110/-DCSupplemental](http://www.pnas.org/lookup/suppl/doi:10.1073/pnas.1302655110/-DCSupplemental).

Using crystallographic, mutational, and biophysical studies, we report here that the relevant Nup54 segment by itself forms a tetrameric helical bundle. Located in the center of this bundle is a patch of highly conserved polar residues, fluidly connected by a hydrogen bond network. Remarkably, the same polar residues of the Nup54 homotetramer also interact with polar residues of Nup58 when forming the Nup54•Nup58 dodecamer. The observed inherent instabilities of these modules (11, 12) would structurally condition them for low-energy barrier transitions between homooligomeric and heterooligomeric states. Hence, we propose that the 64 Nup54 members of a dilated Nup58•Nup54 midplane ring resolve into two rings, each composed of eight Nup54 tetramers; these two Nup54 rings might be stacked upon (or tucked into) the larger Nup58 midplane ring. Together, the tetrameric modules of the three homooligomeric rings reassociate, thereby morphing into a single, large heterooligomeric ring consisting of eight modules of dodecamers. We propose that this ring cycle provides the structural basis for reversibly constricting and dilating the diameter of the central transport channel of the NPC by about 30 nm. Cycling between the three small rings and a single large ring would be regulated in synergy with the unstructured regions of the channel nups (see *Discussion*).

## Results

**Structure of Nup54.** Each of the three “channel” nups, Nup58, Nup54, and Nup62, contains a predicted  $\alpha$ -helical region of about 200 residues. Systematic biochemical mapping experiments revealed that each helical region is at least “divalent” (Fig. 1), i.e., composed of at least two spatially separated domains that are likely distinct binding sites. Uniquely, both of the two binding valences of Nup54, by forming specific interactions with Nup58 and Nup62, are directly involved in the formation of the central transport channel (Fig. 1 and Fig. S14) (12), whereas in the case of Nup58 and Nup62, a second binding valence (indicated by green and yellow bars, respectively, in Fig. 1) is not saturated by the channel nups.

The Nup54•Nup58 interaction (Fig. S14) was previously shown to be dynamically unstable (12). Having already established atomic structures for the Nup58•Nup54 complex (12) and the relevant Nup58 fragment by itself (11), we embarked on elucidating the atomic structure of the relevant Nup54 fragment, with the expectation that such data would allow further refinement of our model of the central transport channel.

The relevant Nup54 fragment (residues 453–494) formed a tetramer, based on its molar mass in solution. For these experiments, Nup54 was separated by size exclusion chromatography and its

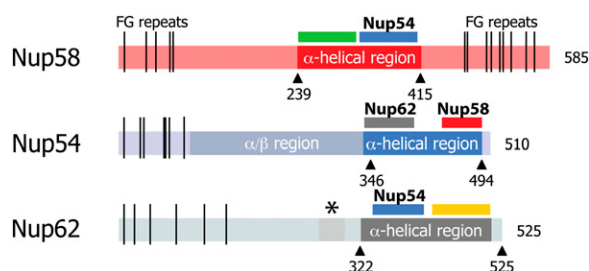


**Fig. 1.** Interaction domains of channel nups. Domain representation of Nup58 (red), Nup54 (blue), and Nup62 (gray) from *Rattus norvegicus* indicating  $\alpha$ -helical (saturated color, bordering residues are indicated by solid triangles),  $\alpha/\beta$  (labeled), and unstructured regions (light shade of color) with FG repeats (black lines) (11). Mapped interacting domains of each channel nup are marked by a bar in the color of the respective interacting partner and labeled (12). Unsaturated “valences” of Nup58 and Nup62 are marked by a green and yellow bar, respectively. A glycosylation region of Nup62 (see *Discussion*) is marked by an asterisk (Fig. S14).

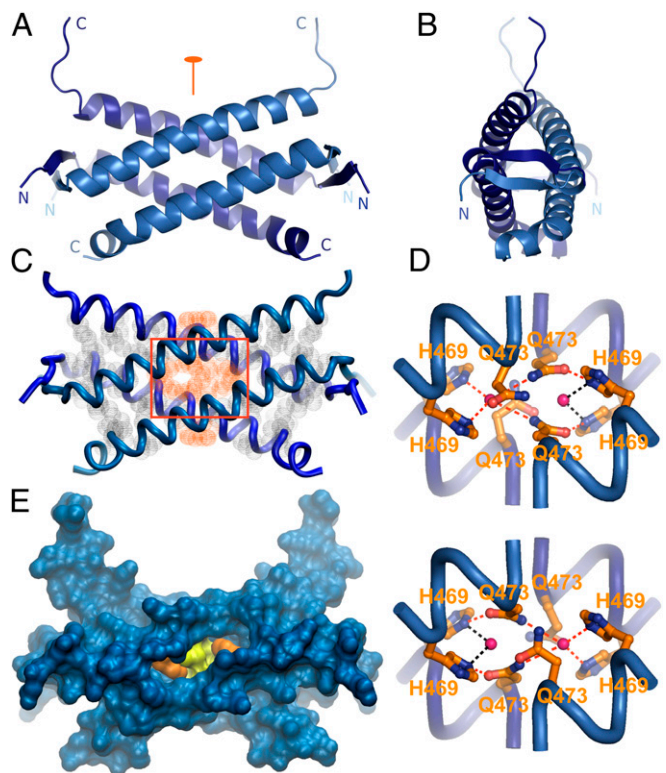


**Fig. 2.** Structure of Nup54. (A and B) Cartoon representation of the Nup54 tetramer (blue), related by a 90° rotation. A twofold axis of symmetry is indicated (orange). Helix I and II conformers are located at the top and bottom of the tetramer, respectively. (C) Ribbon representation of Nup54. Residues that mediate hydrophobic (gray) and polar (orange) interactions in the tetramer are shown in van der Waals sphere representation. (D) Cross-section of the tetrameric interface of Nup54 (boxed in C). A small cluster of polar residues, H469 and Q473 (orange; water molecules as pink spheres), forms a dynamic network of polar hydrogen bonds (red or black dashes). Note that H469 can only form one hydrogen bond at a time (black or red dashes). Furthermore, Q473 has two alternative conformations, shown in the upper and lower panels, respectively. (E) Surface representation of the Nup54 tetramer (blue). Residues H469 and Q473 are highlighted in orange and yellow, respectively. See also Fig. S2.

molar mass was determined by multiangle light scattering (Fig. S1B). The obtained molar mass of Nup54 is similar at various protein concentrations ( $20.1 \pm 0.04$  and  $19.7 \pm 0.04$  kDa, at 2 and 20 mg/mL, respectively) and matches closely to the calculated molar mass of a Nup54 tetramer (21.6 kDa).

The structure of the Nup54 tetramer was determined by single-wavelength anomalous dispersion (SAD) using selenomethionine-derivatized crystals in the space group P6<sub>1</sub>22. To introduce selenomethionine sites, two Ile residues were mutated into Met (see *Materials and Methods*). The final model was refined to 1.5-Å resolution with an  $R_{\text{work}}$  of 19.2% and an  $R_{\text{free}}$  of 22.3% (Table S1).

The Nup54 fragment forms a bundle of four  $\alpha$ -helices, which is composed of two asymmetric units related by a twofold axis of symmetry. Each asymmetric unit consists of two conformers, Helix I and Helix II, which are arranged in an antiparallel fashion (Fig. 2A). In Helix I, a long  $\alpha$ -helix (residues 460–488) is followed by a short coil of six C-terminal residues. In Helix II, the C-terminal four residues are disordered (Fig. S24). At the N terminus, both conformers display a “hook” composed of a short  $\beta$ -strand at an about 90° angle to the helical axis (Fig. 2A and B and Fig. S3A and B). Two strands (or “hooks”), one from Helix I and one from Helix II from the neighboring asymmetric unit, form an antiparallel  $\beta$ -sheet. Two  $\beta$ -sheets surround the

helical bundle. Because of their low B factor, they probably help to rigidify the tetramer and act as “braces.” The four-helix bundle buries a solvent accessible area of 6,230 Å<sup>2</sup> and measures 50 Å in length, 29 Å in height, and 20 Å in depth (Fig. S4C).

**Buried Polar Residues as a Prominent Feature of Nup54 Homotetramer.** The Nup54 tetramer is mainly held together by nonpolar van der Waals interactions (Fig. 2C). A buried cluster of polar residues is located in a cavity at the center of the homotetramer (boxed in Fig. 2C). This cluster consists of residues Q473 and H469 from the four Nup54 protomers, which are connected by a network of polar hydrogen bonds that contains two bridging water molecules (Fig. 2D). In the structure, two alternative conformations of Q473 are observed, illustrating the conformational flexibility of Q473 and resulting in multiple different hydrogen bond networks (Fig. 2D). The cavity in which the polar residues are located protrudes from a deep cleft in the surface of the tetramer and results in exposure of H469 and Q473 to bulk solvent (Fig. 2E).

A sequence alignment reveals that both H469 and Q473 are well conserved (Fig. S24). Mapping the degree of conservation on the structure reveals that these residues belong to a region in the center of the helical bundle that is the most highly conserved of the Nup54 tetramer (Fig. S2), suggesting physiological relevance of this portion of the tetrameric interface. This central region is accessible to bulk solvent and likely provides an element of instability to the Nup54 homotetramer.

**Structure of the Nup54 Homooligomer Can Be Stabilized by Mutagenesis.** The role of buried polar residues for the stability of the Nup54 tetramer formation was analyzed by mutagenesis. The central cavity containing H469 and Q473 is loosely packed as indicated by the alternative hydrogen bond networks formed by Q473, H469, and bridging water molecules.

To reduce the exposure of the interface to the bulk solvent, and thus to stabilize the homotetramer, these residues were replaced by nonpolar ones. Variants H469F and H469F/Q473L of Nup54 were made and their stability was probed by circular dichroism (CD) spectroscopy. CD wavelength spectra of  $\alpha$ -helical proteins show characteristic minima at 208 and 222 nm. The CD spectra of Nup54 wild-type (wt) and variants H469F and H469F/Q473L at 8 °C indicate  $\alpha$ -helical structures and are very similar (Fig. 3A). In thermal unfolding profiles, recorded by CD spectroscopy at 222 nm, Nup54 wt and the H469F variant both display sigmoidal curves suggesting a single transition between helix and random coil conformations. The resulting melting temperature ( $T_m$ ) of the H469F mutant is 88.2  $\pm$  1.1 °C, compared with 62.5  $\pm$  1.3 °C for the wt protein (Fig. 3B). Strikingly, the H469F/Q473L variant failed to provide a typical melting curve and a plateau is not reached, suggesting that this variant exhibits an extremely stable  $\alpha$ -helical structure. To validate this observation, CD wavelength spectra were recorded at 8 °C and 100 °C. The wt displays the characteristic minima of  $\alpha$ -helical structures only at 8 °C, but not at 100 °C, indicating unfolding (Fig. 3C). However, CD spectra recorded for the H469F/Q473L variant are very similar at 8 °C and 100 °C (Fig. 3D), indicating that the H469F/Q473L variant is thermostable and forms Nup54 homooligomers with extreme structural stability compared with the wt. These results confirm that H469 and Q473 contribute an element of inherent instability to the Nup54 homotetramer.

**Structure Comparison of the Nup54 Homotetramer and the Nup54•Nup58 Complex.** Previously, the structure of the Nup54•Nup58 interacting domain was determined (residue 445–494 of Nup54 and 327–415 of Nup58) (12). Because the N-terminal residues of Nup54 are disordered in the structure (residues 445–455), subsequent studies of Nup54 were performed with a shorter fragment of Nup54 (residues 453–494).

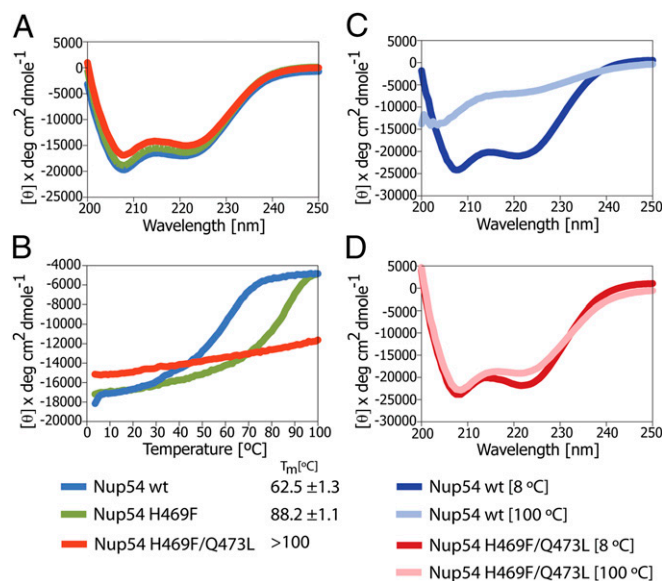


**Fig. 3.** CD spectroscopy analysis of Nup54 and its variants. (A) CD wavelength spectra of Nup54 wild-type (wt) (blue) and its variants H469F (green) and H469F/Q473L (red) at 8 °C. The mean residue molar ellipticity  $[\theta]$  versus the wavelength is shown. (B) Thermal melting curves of Nup54 wt and its variants H469F and H469F/Q473L, monitored by CD spectroscopy at 222 nm. Unfolding is monitored by the increase of  $[\theta]$  as a function of temperature. The resulting melting temperatures  $T_m$  are indicated. (C and D) CD wavelength spectra at 8 °C and 100 °C of (C) Nup54 wt (blue, light blue) and (D) Nup54 H469F/Q473L (red, pink).

In the crystal structure, Nup54•Nup58 forms a higher order oligomer in the shape of a spiral, which can be relaxed to a flexible ring (12). The repeating module of the spiral is a dodecamer (see below; Fig. 4A and Fig. S44). We propose that eight such dodecamers form a ring in the eightfold symmetric NPC (see below; Fig. 4E). In the Nup54•Nup58 structure, Nup54 exhibits two conformations: a straight one with a single  $\alpha$ -helix (Fig. S3C) and a bent conformer of two  $\alpha$ -helices, which are connected by a central loop (Fig. S3D) (12). Together with the structure of the Nup54 homotetramer, these structures show that Nup54 exhibits large conformational plasticity.

Strikingly, in the Nup54 homooligomer, a  $\beta$ -sheet is formed in the N-terminal region, whereas these residues do not assume a regular secondary structure in both Nup54 conformers of the Nup54•Nup58 complex (Figs. S3 A–D and S24). The central  $\alpha$ -helical regions of Helix I and Helix II resemble the conformation observed in the straight Nup54 conformer of Nup54•Nup58. However, in the C-terminal part of Helix I and II, residues 489–493 do not assume a regular secondary structure, whereas they are  $\alpha$ -helical in the straight conformer of Nup54 (Fig. S24). In summary, Nup54 displays conformational plasticity and multiple regions that can undergo secondary structure transitions.

A buried polar cluster of residues H469 and Q473 plays a role in the stability of the Nup54 homotetramer. In the Nup54•Nup58 complex, H469 and Q473 of the straight Nup54 conformer form a hydrogen bond network with residue Y346 of Nup58 (Fig. S3E). This buried polar cluster is surrounded by a hydrophobic interface and partially accessible to the bulk solvent by a small cleft (Fig. S3F), as similarly observed in the homotetramer (Fig. 2E).

Polar residues have a generally destabilizing effect in hydrophobic interfaces, while at the same time they impart specificity on protein–protein interactions, due to the requirements for complementarity of side-chain stereochemistry (13, 14). Hence, pairing of polar residues in hydrophobic interfaces is important for selection of interacting proteins. Our structural analysis suggests

that residues H469 and Q473 of Nup54 are important for the specificity of interactions in the Nup54 homotetramer (Fig. 2*D*) and in the Nup54•Nup58 complex. Furthermore, in the Nup54•Nup58 complex, Q473 forms a polar hydrogen bond with Y346 of Nup58 (Fig. S3*E*). In the Nup58 homotetramer (11), the same residue (Y346) mediates a buried polar hydrogen bond with Y346 from another Nup58 molecule (12). A swap of polar partners as observed in these structures can potentially lead to tertiary structural changes (15), because polar interactions are often crucial to imparting a unique structure to helix–helix interfaces (13–15).

The negative effect of these polar residues on the stability of the Nup54 homotetramer is documented by the increased thermal stability of the H469F/Q473L variant compared with the wild type (Fig. 3). The instability of the Nup54 homotetramer may partly explain why in solution the interaction between Nup54 and Nup58 is dynamic and the Nup54•Nup58 complex spontaneously undergoes disassembly and reassembly (12).

Furthermore, the polar residues in the core of the Nup54 homotetramer as well as in the Nup54•Nup58 complex are partially accessible to bulk solvent by cavities (Fig. 2*E* and Fig. S3*F*). This increases the probability of solvation of these residues, leading to an increase of the local dielectric and a weakening of the interhelix interactions. This may ultimately facilitate dissociation of the assemblies. The fact that these polar residues are conserved (Fig. S2) suggests that the inherent instability of this interface is physiologically significant for the Nup54•Nup58 complex and the Nup54 homotetramer. This architecture may explain the dynamic interaction of Nup54 and Nup58 and suggests that these residues play a role in structural transitions (as observed for example in ref. 15).

## Discussion

We present here structural, mutational, and biophysical analyses on a segment of Nup54, which can either bind to a segment of Nup58 or exist in a free form. Our data here show that the free Nup54 segment tetramerizes to form a helical bundle. The homotetramer is largely held together by hydrophobic van der Waals forces, but contains a central patch of conserved polar residues that are linked to each other by a fluid hydrogen bond network. Mutational analyses showed that these residues provide dynamic instability to the Nup54 tetramer. Collectively, the previously observed intrinsic instabilities of a Nup58 homooligomer (11) and a Nup54•Nup58 heterooligomer (12), as well as the built-in instability of the Nup54 homotetramer reported here, may “condition” these structures for reversible transition across low energy barriers. A gallery summarizing the X-ray structures of the homooligomeric and heterooligomeric modules of Nup54 and Nup58 is shown in Fig. 4*A–C*.

**Ring Cycle for the Dilated and Constricted Transport Channel.** Guided by established axes of symmetry of the core of the NPC, twofold in midplane and eightfold in the nucleocytoplasmic direction (2), we placed the three atomic structures shown in Fig. 4*A–C* (see also Fig. S4), each into a ring consisting of eight modules. This exercise gave rise to the idea of a “ring cycle” (Movie S1), in which a single large Nup58•Nup54 ring [~40- to 50-nm diameter; Fig. 4*E* (12)] is resolved into three smaller rings, one of Nup58 and two of Nup54 (Fig. 4*F*). The Nup58 ring of ~20-nm diameter was placed into midplane because of its twofold symmetry (11, 12). The two Nup54 rings were tentatively placed above and below the midplane Nup58 ring (Fig. 4*F*). However, the smaller dimensions of the Nup54 ring (~10-nm diameter; Fig. S5) would also permit both Nup54 rings to be tucked into the larger Nup58 ring, as indicated in Fig. S5 (see also Fig. S4). In accordance with our previous proposals (12), we suggest that the single and large Nup54•Nup58 ring represents the dilated form of the central midplane ring, whereas the three smaller rings, two Nup54 rings

and one Nup58 ring, represent the constricted form of the midplane ring. As previously pointed out (12), the large ring, because of lateral sliding along its hydrophilic intramodular interfaces in midplane, is expandable to ~50-nm diameter; and, as also pointed out previously (12), a local, intramodular derailment could even open a “lateral gate” for transport of integral membrane proteins from the outer to the inner membrane of the nuclear envelope (16). In essence, in our ring cycle model for dilated and constricted states of midplane rings, 96 segments of Nup58 and Nup54 form a large and single Nup58•Nup54 midplane ring and can be reassorted into three smaller rings (of 32 segments each), one of Nup58 and two of Nup54. In accordance with our previous proposals (12), the ring cycle can be regulated and thereby be coupled to intracellular demands for transport.

**Regulation of the Ring Cycle.** Because of an up-and-down projection of the Nup54 linker region (Fig. 1 and Fig. S14) from the midplane ring(s), the “finger”-shaped triple helices (Fig. 4*D*), each formed by the previously described Nup54•Nup62 interactome, were placed at the cytoplasmic and nucleoplasmic entries to the midplane ring (12). Fig. 4*G* and *H* show the placement of the “fingers” in the dilated and constricted midplane ring. Although we have so far not detected an interaction between the finger regions, it is likely that crowding of 32 such fingers, each above and below the constricted midplane rings, may contribute to a closed state (Fig. 4*G* and *H* and Fig. S5).

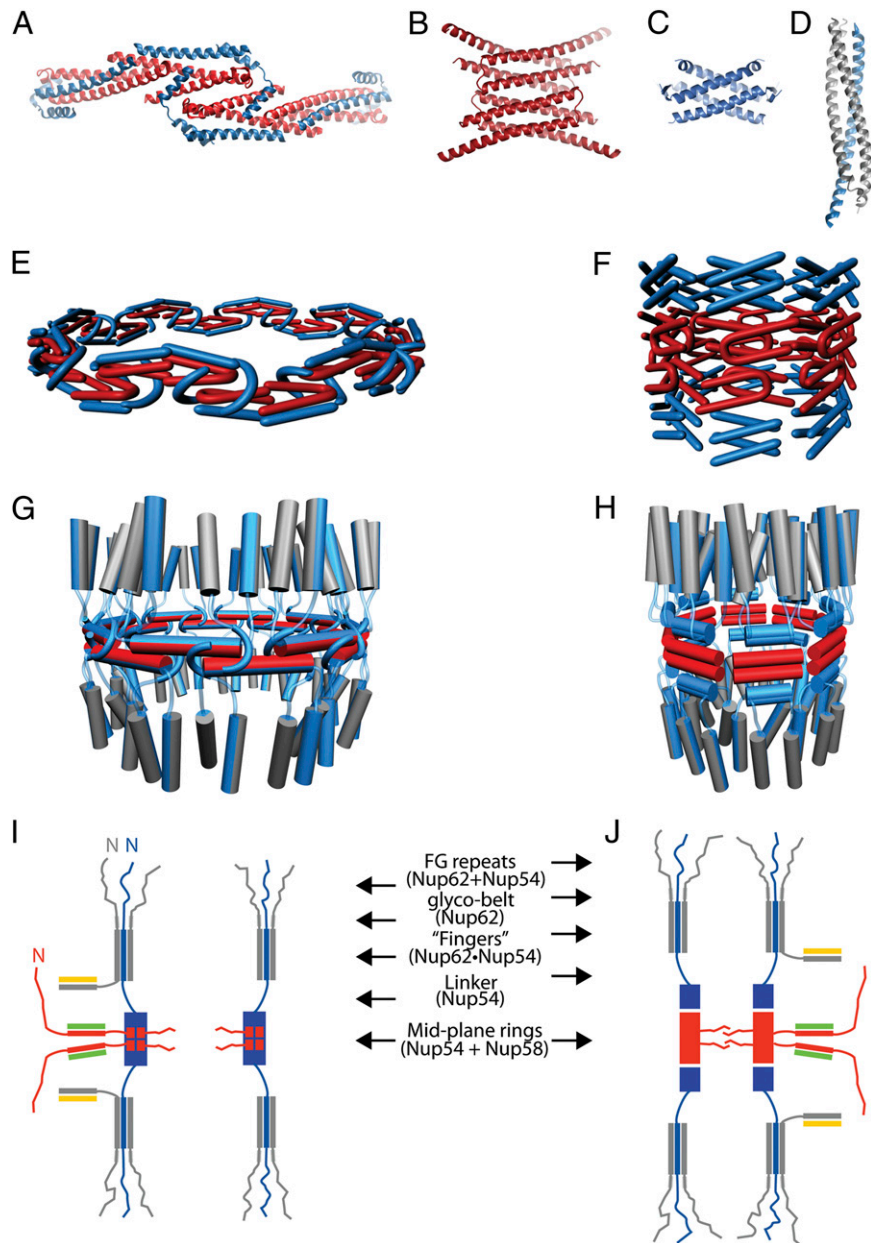
The finger-shaped triple helix not only bundles but also aligns one Nup54 and two Nup62 molecules, before splitting into “unstructured” appendages (Fig. 4*I* and *J*, see also Fig. 1). At the N-terminal end of each of these appendages are FG-repeat motifs, which are known to function as binding sites for [cargo•transport-factor] complexes (8).

Especially noteworthy is that each Nup62 molecule, between the fingertip and N-terminal FG repeats, displays a heavily glycosylated region, each of which contains 10 single GlcNAc residues, linked to a Ser (Thr) residue (17, 18). The physiological significance of what we termed the “glyco-belt” region (Fig. 4*I* and *J*) is presently not known. As those Ser (Thr) residues can be enzymatically deglycosylated and potentially be phosphorylated (19), modification of these regions may play important, yet-to-be-elucidated roles in NPC function and/or assembly (20). Like the fingers, in the constricted form of the pore, these glycosylated residues would be more crowded and could enhance cohesion in the constricted state of the pore (Fig. 4*I* and *J*). Interestingly, GlcNAc modifications do not occur in yeast so that the Nsp1 homolog of mammalian Nup62 lacks a glyco-belt. Of note, and in contrast to mammalian Nup62, yeast Nsp1 contains over 30 FG repeats per molecule, as opposed to only 6 per Nup62 molecule. The significance of these differences is presently unknown as well.

Because FG repeats of Nup62 and Nup54 are anchored to the fingertips, they are located some distance away from the midplane ring. In contrast, the C-terminal FG repeats of Nup58 are likely to project directly to the center of the midplane ring (Fig. 4*I* and *J*). Because of this “privileged” location, the Nup58 C-terminal FG repeats could exert a critical function in our “ligand-gating” model for the nuclear pore by [cargo•transport-factor] complexes (see below). Of note, the yeast homolog of vertebrate Nup58, Nup49, does not contain C-terminal FG repeats and therefore ligand gating of a putative yeast midplane ring may be regulated by FG repeats of the other channel nups. It remains to be determined whether the structured regions of yeast homologs form modules similar to those determined for the vertebrate channel nups.

The complete tracing of the three channel nups of vertebrates in our model shown in Fig. 4*I* and *J* places the N-terminal FG repeat of Nup58 facing away from the channel. The rationale for placing the N-terminal FG repeat outside the central channel is based on our conjecture that another segment in the helical

**Fig. 4.** Ring cycle for dilating and constricting the nuclear pore. (A–D) Summary of modules of determined X-ray structures of segments derived from channel nucleoporins Nup54, Nup58, and Nup62 (Fig. 1). (A) Nup54•Nup58 dodecamer consisting of eight Nup54 (blue) and four Nup58 (red) protomers; note the “bent” and “straight” conformers of the Nup54 protomer (12). (B) Nup58 homotetramer; each protomer consists of a helical hairpin (11). (C) Nup54 homotetramer with two distinct conformers of the Nup54 protomer (Fig. S3 A and B). (D) Nup62•Nup54 triple helix (12), with two protomers of Nup62 in gray and one protomer of Nup54 in blue. For visual simplification, the structural elements of the modules are schematically modified in E–J. (E and F) We propose that eight of each of the modules shown in A–C form a ring, representing dilated and constricted states. (E) In the dilated state, eight Nup54•Nup58 dodecamers form a mid-plane ring, the diameter of which is flexible in the range between 40–50 nm as a result of intramolecular sliding (12). (F) For constricting the pore, the 96 constituent protomers of the dilated mid-plane ring resolve into three homooligomeric rings of 32 protomers each; because of its twofold symmetry, the Nup58 ring is placed in midplane (11), whereas the two Nup54 rings are tentatively placed below and above (F) or tucked within the Nup58 ring (Fig. S5). The three homooligomeric rings, stacked in midplane, display a diameter in the 10- to 20-nm range (Figs. S4 and S5). (G and H) Finger attachments to the dilated midplane ring (G) and to the two Nup54 rings in the constricted state (H): A flexible linker region of Nup54, indicated as blue transparent tube, continues into a Nup62•Nup54 triple helix (D), simplified to a vertically oriented, blue and gray cylinder and termed finger; note the presence of a total of 64 fingers, 32 each on the nucleoplasmic and cytoplasmic sides; cycling from a dilated to a constricted state (G to H) increases crowding of fingers. (I and J) Schematic tracing of full-length channel nups (Fig. 1) in a vertical slice across the dilated (I) and constricted (J) state; distinct nup regions are labeled (see text) and indicated by arrows; color-coded N depicts the N terminus in one each of three channel nups; an “unsaturated valence” of Nup62 (only one of two is indicated) and of Nup58 for a yet-to-be-identified segment of another nup, is indicated by a yellow and a green bar, respectively (Fig. 1); note location of the two FG repeats of Nup58: C-terminal FG repeat projects to the center of the midplane ring, whereas the N-terminal FG repeat projects away from the pore, suggesting that it may bind to a solenoid nucleoporin in the surrounding of the central transport channel. Tracing the path of all three channel nucleoporins, Nup58, Nup54, Nup62, through a single transport channel of the NPC, in copies of 32:64:128 (12), indicates that the three channel nups not only line the channel but also anchor it to the surrounding matrix of nups. Anchorage would be accomplished by 128 binding sites emanating from Nup62, at the base of the fingers, and by 32 binding sites from the Nup58 midplane ring.



region of Nup58 (Figs. 1 and 4 I and J, green bar) interacts with a segment of another nup located peripherally to the midplane ring (12, 21, 22). However, this interaction has yet to be characterized. The N-terminal FG repeats of Nup58, here placed outside the transport channel, may bind to a solenoid region of a peripheral nup (23), rather than to an equivalent solenoid region of a typical [cargo•transport-factor] complex. This may help to further reinforce the large network of interactions between nups in the NPC.

Our tracing of each of the three channel nups in the model shown in Fig. 4 also places the position of a second segment of the helical region of Nup62 (Figs. 1 and 4 I and J, yellow bars) to a yet-unidentified nup that our model positions peripheral to the midplane-ring-connected fingers (12). By analogy to yeast binding

studies, an N-terminal segment of Nup93 is a possible candidate for such an interaction (21, 22). Hence two specific segments, one from Nup58, the other one from Nup62, appear to be dedicated in anchoring the midplane ring or their attached fingers, respectively.

The FG repeats of channel nups, as well as of other nups, have been at the center of numerous studies and led to several models of their function (for a review, see ref. 7). However, a common denominator of these models is that the structured regions of nups merely provide a static scaffold and line a central cylinder-like space, whereas FG repeats, projecting into the cylinder center and up and down into the cytoplasm and nucleoplasm, are the principal regulators of nucleo-cytoplasmic transport. Our ring cycle model, in which two distinct helical regions of Nup54

and Nup58 are differentially bundled into modules that can undergo rearrangements to form repetitive modules for three smaller rings or a single large ring, embodying constricted and dilated forms of a midplane ring, represents a paradigm shift of how a central transport cylinder is built. Instead of about a dozen nups lining such a central transport conduit (6), our model suggests that altogether only four distinct segments of three channel nups are lining the channel, whereas two other segments of channel nups Nup58 and Nup62 are anchoring it to surrounding nups (Fig. 4 I and J) (12).

In our ring cycle model, FG repeats function in synergy with structured portions of channel nups to control dilation and constriction of the midplane ring and their attachments. For example, as ligand binding sites for [cargo•transport-factor] complexes, they may function in stabilizing the modules of dilated midplane pores, acting as yin. In their unoccupied state, they could, as yang, reinforce the constricted state of the midplane ring(s) by crowding the finger region and weakly interacting with each other (Fig. 4 I and J).

As is the case for any model, several aspects of our ring cycle model await experimental scrutiny. For example, higher order ring structures have yet to be assembled. However, in vitro assembly of stable rings may require fragments of the channel nups, larger than those that have been trimmed down to the minimally interacting fragments that were optimized for crystallization. As an additional challenge, in vitro assembly of stable rings may require participation of surrounding nups. Likewise, the idea of ligand gating, based on synergy of FG repeats with the structured regions of the channel nups, has yet to be scrutinized by biophysical approaches.

In conclusion, in our ring cycle model, four distinct pieces of three channel nups, Nup58, Nup54, and Nup62, form repetitive modules that can assemble into three small rings or into a single large ring, with attached finger-like structures, representing dilated and constricted forms of the central transport cylinder of the NPC. The ring cycle is regulated by terminal FG repeats of

channel nups, thereby linking a cell's ratio of dilated to constricted nuclear pores to transport demand.

## Materials and Methods

A detailed description of the methods can be found in *SI Materials and Methods*.

**Protein Expression and Purification.** Expression constructs of Nup54, residues 453–494 from *Rattus norvegicus*, were generated and expressed from the pET28a vector as described (11, 12). Proteins were purified by His<sub>6</sub>-affinity chromatography, followed by thrombin cleavage, anion exchange chromatography, and size exclusion chromatography, as described (11, 12).

**Crystallization, Data Collection, and Structure Determination of Nup54.** Crystals of a selenomethionine-derivatized, purified Nup54 variant I458M I481M (residues 453–494) were grown at 20 °C in hanging drop setups. X-ray data were collected at beamline x29A of the National Synchrotron Light Source at Brookhaven National Laboratory (Upton, NY), at 100 K, from a single crystal in space group P6<sub>2</sub>2. Phases were obtained from a selenomethionine SAD diffraction dataset. Data collection and refinement statistics are summarized in Table S1.

**CD Spectroscopy.** For analysis of thermal unfolding profiles, a two-state denaturation model ( $\alpha$ -helix to random coil) was used. The apparent melting temperature ( $T_m$ ) was determined from the peak of differential melting curves  $d[\theta_{222}]/dT$ .

**ACKNOWLEDGMENTS.** We thank Janisha Biyanwila-Kukreja for excellent technical assistance. X-ray data were collected at beamline X29A of the National Synchrotron Light Source (NSLS) at Brookhaven National Laboratory (Upton, NY) [initial data at beamline 8.2.1 at the Advanced Light Source (ALS) (Berkeley, CA)]. We thank Wuxian Shi (NSLS) and Corie Ralston (ALS) for their outstanding support, The Rockefeller University structural biology and high-throughput screening resource centers for access to instrumentation, Deena Oren and Antonio Luz for their excellent support, Elias Coutavas and Radha Chauhan for helpful discussions, Joseph Alexander for artwork, Alok Sharma, Richard A. Wing, Junseock Koh, B. Blus, and E. Coutavas for critically reading the manuscript, and David King (Howard Hughes Medical Institute, Berkeley, CA) for mass spectrometry analysis.

- Liu X, Mitchell JM, Wozniak RW, Blobel G, Fan J (2012) Structural evolution of the membrane-coating module of the nuclear pore complex. *Proc Natl Acad Sci USA* 109(41):16498–16503.
- Hoelz A, Debler EW, Blobel G (2011) The structure of the nuclear pore complex. *Annu Rev Biochem* 80:613–643.
- Beck M, et al. (2004) Nuclear pore complex structure and dynamics revealed by cryo-electron tomography. *Science* 306(5700):1387–1390.
- Feldherr CM, Akin D (1990) The permeability of the nuclear envelope in dividing and nondividing cell cultures. *J Cell Biol* 111(1):1–8.
- Kiseleva E, Goldberg MW, Allen TD, Akey CW (1998) Active nuclear pore complexes in *Chironomus*: Visualization of transporter configurations related to mRNP export. *J Cell Sci* 111(Pt 2):223–236.
- Alber F, et al. (2007) The molecular architecture of the nuclear pore complex. *Nature* 450(7170):695–701.
- Tetenbaum-Novatt J, Rout MP (2010) The mechanism of nucleocytoplasmic transport through the nuclear pore complex. *Cold Spring Harb Symp Quant Biol* 75:567–584.
- Radu A, Moore MS, Blobel G (1995) The peptide repeat domain of nucleoporin Nup98 functions as a docking site in transport across the nuclear pore complex. *Cell* 81(2):215–222.
- Guan T, et al. (1995) Structural analysis of the p62 complex, an assembly of O-linked glycoproteins that localizes near the central gated channel of the nuclear pore complex. *Mol Biol Cell* 6(11):1591–1603.
- Hu T, Guan T, Gerace L (1996) Molecular and functional characterization of the p62 complex, an assembly of nuclear pore complex glycoproteins. *J Cell Biol* 134(3):589–601.
- Melčák I, Hoelz A, Blobel G (2007) Structure of Nup58/45 suggests flexible nuclear pore diameter by intermolecular sliding. *Science* 315(5819):1729–1732.
- Solmaz SR, Chauhan R, Blobel G, Melčák I (2011) Molecular architecture of the transport channel of the nuclear pore complex. *Cell* 147(3):590–602.
- Gonzalez L, Jr., Woolfson DN, Alber T (1996) Buried polar residues and structural specificity in the GCN4 leucine zipper. *Nat Struct Biol* 3(12):1011–1018.
- Koder RL, et al. (2006) Nativelike structure in designed four alpha-helix bundles driven by buried polar interactions. *J Am Chem Soc* 128(45):14450–14451.
- Wang J, Sykes BD, Ryan RO (2002) Structural basis for the conformational adaptability of apolipoprotein III, a helix-bundle exchangeable apolipoprotein. *Proc Natl Acad Sci USA* 99(3):1188–1193.
- King MC, Lusk CP, Blobel G (2006) Karyopherin-mediated import of integral inner nuclear membrane proteins. *Nature* 442(7106):1003–1007.
- Holt GD, et al. (1987) Nuclear pore complex glycoproteins contain cytoplasmically disposed O-linked N-acetylglucosamine. *J Cell Biol* 104(5):1157–1164.
- Lubas WA, Smith M, Starr CM, Hanover JA (1995) Analysis of nuclear pore protein p62 glycosylation. *Biochemistry* 34(5):1686–1694.
- Hart GW, Slawson C, Ramirez-Correa G, Lagerlof O (2011) Cross talk between O-GlcNAcylation and phosphorylation: Roles in signaling, transcription, and chronic disease. *Annu Rev Biochem* 80:825–858.
- Davis LI, Blobel G (1986) Identification and characterization of a nuclear pore complex protein. *Cell* 45(5):699–709.
- Grandi P, Schlaich N, Tekotte H, Hurt EC (1995) Functional interaction of Nic96p with a core nucleoporin complex consisting of Nsp1p, Nup49p and a novel protein Nup57p. *EMBO J* 14(1):76–87.
- Bailer SM, Balduf C, Hurt E (2001) The Nsp1p carboxy-terminal domain is organized into functionally distinct coiled-coil regions required for assembly of nucleoporin subcomplexes and nucleocytoplasmic transport. *Mol Cell Biol* 21(23):7944–7955.
- Schrader N, et al. (2008) Structural basis of the nic96 subcomplex organization in the nuclear pore channel. *Mol Cell* 29(1):46–55.